Stability Analysis of Multiple Grid-Connected Inverters Using Different Feedback Currents

David Carballo, Edgar Escala and Juan Carlos Balda
Department of Electrical Engineering
University of Arkansas at Fayetteville
Fayetteville, Arkansas, USA
email: dmcarbal@uark.edu,eaescala@uark.edu, jbalda@uark.edu

***Abstract*—Distributed generation is gaining greater penetration levels in distribution grids due to government incentives for integrating distributed energy resources (DERs) and DER cost reductions. The frequency response of a grid-connected single inverter changes as other inverters are connected in parallel due to the couplings among grid inductance and/or inverter output filters. The selection of the inverter- or grid-side currents as feedback control signals is then not trivial because each one has tradeoffs. This paper analyses the system stability for multiple parallel- and grid-connected inverters using the inverter- or grid-side currents as feedback signals. Modeling of both feedback signals is performed using the current separation technique. Morover, the stability range for different conditions including active damping is analyzed through the root locus technique. The grid-side current has a wider range of stability, but the inverter-side current allows for higher values of the proportional gain near the critical frequency and no extra sensors are needed since measurement of the inverter current is needed for protection in high-power applications.**

Keywords— Grid-connected inverters, LCL filters, multiparallel inverters, stability anaylses, current control.

I. INTRODUCTION

Microgrids have several advantages like effective integration of distributed energy resources (DERs) into distribution networks to allow for bidirectional power flows, and reduced transmission and distribution losses. Interfaces between DERs and microgrids are often based on power converters (inverters) with LCL filters that provide a higher damping capability (-60 dB/dec) in comparison with a simple L filter (-20 dB/dec) [1]. However, LCL filters introduce resonance issues that can cause current-controller instability and that can become more severe as more power electronics devices are connected to the grid [2]. The scenario becomes more challenging when DER converters of higher power ratings are used while the voltage levels remain in the low-voltage range (208 V ~ 480 V). This results in a much smaller base impedance value on a per-unit (p.u.) basis, making the filter inductor values on the same order as the grid impedance and, thus, increasing the possibility of any instability issue caused by coupling between inverter and grid impedances [1]. Therefore, a stability analysis of the potential interactions between several parallel LCL filters and their effects on current controllers is crucial for satisfactory system performance.

978-1-5386-6705-7/18/$31.00 ©2018 IEEE

Either the grid- or inverter-side currents can be selected for feedback in a DER current controller. While grid-side currents are usually selected because of direct control of the grid-injected currents, using the inverter-side currents may present some advantages like faster fault current interruption and an inherent damping term in the transfer function [3-4]. The authors of [5] performed a comparison that demonstrated tradeoffs when using these two current-control approaches for only a single inverter. Although the authors of [6-7] presented an analysis on the range of the proportional gain of the current controller for multiple grid-connected inverters, they only considered the grid-side currents for feedback purposes. The work presented here expands upon the stability analysis in [4-8] to evaluate the stability regions for multiple grid-connected inverters when using the inverter-side currents for feedback with the main goal of determining tradeoffs between these two current-feedback approaches.

This paper is organized as follows: Section II presents an overview of the modeling of the inverter- and grid-side currents, Section III evaluates the system stability with and without the use of active damping, Section IV analyzes simulation results, and Section V provides the main conclusions.

II. MODELING OF THE PARALLEL INVERTERS

A. Inverter-Side Current − Mathematical Modeling

Multiple paralleled grid-connected inverters are illustrated in Fig. 1, where Z_1 and Z_2 are the s-domain impedances of the inverter- and grid-side filter inductances, Z_3 is the filter capacitive impedance, Z_g is the grid impedance, and the second subscript refers to the inverter number. Using the principle of superposition to remove the influence of the grid and the other inverter voltages, and assuming that the inverters are equal (i.e., same LCL filter parameters), the inverter-side currents i_{1j} (j=1, 2,..n) with respect to the inverter voltages can be written as:

$$\begin{pmatrix} i_{11} \\ i_{12} \\ \dots \\ i_{1n} \end{pmatrix} = \begin{pmatrix} G_{11} & G_{12} & \dots & G_{12} \\ G_{12} & G_{11} & \dots & G_{12} \\ \dots & \dots & \dots & \dots \\ G_{12} & G_{12} & \dots & G_{11} \end{pmatrix} \cdot \begin{pmatrix} v_{01} \\ v_{02} \\ \dots \\ v_{0n} \end{pmatrix}. \quad (1)$$

where G_{11} and G_{12} are calculated as follows [6]:

$$G_{11} = \frac{n-1}{n} G_{inv} + \frac{1}{n} G_{coupling_{inv}}, \quad (2)$$

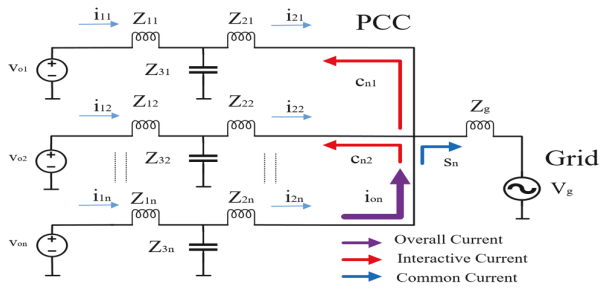

Fig. 1. Schematic of multiple paralleled grid-connected inverters.

$$G_{12} = -\frac{1}{n}G_{inv} + \frac{1}{n}G_{coupling_{inv}}, \quad (3)$$

with G_{inv} the transfer function of the LCL filter and $G_{coupling_{inv}}$ the transfer function including the effects of the grid impedance. Both are presented below:

$$G_{inv} = \frac{(Z_3 + Z_2)}{Z_1Z_2 + Z_1Z_3 + Z_2Z_3} = \frac{s^2 + \omega_0^2}{L_1 s(s^2 + \omega_{res}^2)} \quad (4)$$

$$G_{coupling_{inv}} = \frac{(Z_3 + Z_2 + nZ_g)}{Z_1Z_2 + Z_1Z_3 + Z_2Z_3 + nZ_g(Z_3 + Z_1)} = \frac{s^2 + \omega_{01}^2}{L_1 s(s^2 + \omega_{res1}^2)} \quad (5)$$

where ω_{res} and ω_o are the LCL filter resonance and antiresonance frequencies, and ω_{res1} and ω_{o1} are the resonance and antiresonance frequencies taking into account the coupling with the grid inductance with n paralleled inverters (all in rad/s):

$$\begin{cases} \omega_{res} = 2\pi f_{res} = \sqrt{(L_1 + L_2)/(L_1 L_2 C_f)}, \\ \omega_o = 2\pi f_o = \sqrt{1/(L_2 C_f)}, \\ \omega_{res1} = 2\pi f_{res1} = \sqrt{(L_1 + L_2 + nL_g)/(L_1(L_2 + nL_g)C_f)}, \\ \omega_{o1} = 2\pi f_{o1} = \sqrt{1/((L_2 + nL_g)C_f)}. \end{cases} \quad (6)$$

From (1), the first-inverter-side currents are given by:

$$i_{11} = \frac{1}{n}G_{inv}(v_{01} - v_{02}) + \cdots + \frac{1}{n}G_{inv}(v_{01} - v_{0n}) + \frac{1}{n}G_{coupling_{inv}}(v_{01} + \cdots + v_{0n}) \quad (7)$$

From (7), the inverter-side currents i_{11} have two components: the interactive one which circulates between two inverters and the common one that is injected into the grid, as illustrated in Fig. 1 [6-7].

B. Grid-Side Current – Mathematical Modeling

Following the same process as in the previous section and presented in [6], the grid-side currents i_{2j} $(j = 1,2,..n)$ with respect to the inverter voltages can be written like (1)-(3) but with different transfer functions for the LCL filter and the coupling term:

$$G_{11} = \frac{n-1}{n}G_{grid} + \frac{1}{n}G_{coupling_{grid}} \quad (8)$$

$$G_{12} = -\frac{1}{n}G_{grid} + \frac{1}{n}G_{coupling_{grid}} \quad (9)$$

$$G_{grid} = \frac{Z_3}{Z_1Z_2 + Z_1Z_3 + Z_2Z_3} = \frac{1}{L_1L_2C_f s(s^2 + \omega_{res}^2)} \quad (10)$$

$$G_{coupling_{grid}} = \frac{Z_3}{Z_1Z_2 + Z_1Z_3 + Z_2Z_3 + nZ_g(Z_3 + Z_1)} = \frac{1}{sL_1C_f(L_2 + nL_g)(s^2 + \omega_{res1}^2)} \quad (11)$$

Like (7), the first-grid-side currents can be expressed as:

$$i_{21} = \frac{1}{n}G_{grid}(v_{01} - v_{02}) + \cdots + \frac{1}{n}G_{grid}(v_{01} - v_{0n}) + \frac{1}{n}G_{coupling_{grid}}(v_{01} + \cdots + v_{0n}) \quad (12)$$

comprising interactive and common currents shown in Fig. 1.

III. Stability Analysis and Active Damping

A. Control Strategy

The block diagram of a single current-control loop for the inverter-side current feedback in the s-domain is presented in Fig. 2 (a). In the figure, i_1^* represents the reference current commanded to the controller, G_{d-DSP} the DSP computational delay, K_{pwm} the linear response of the inverter with gain of $K_{pwm} = V_{dc}/\sqrt{3}$ for a space vector modulation implementation, and G_{PI} the PI controller chosen in this paper:

$$G_{PI}(s) = K_P + \frac{K_i}{s} \quad (13)$$

The current controller in Fig. 2 (a) as modeled in the z-domain is in Fig. 2 (b) since the DSP is a discrete system. In the figure, the PI controller in (13) is discretized by applying a Tustin transform with prewarping while a zero-order-hold (ZOH) transform is applied to the transfer function of the LCL filter [2]. Moreover, a sample delay z^{-1} accounts for the delay of the DSP. Although both figures are shown using the inverter-side current as reference, the same control diagram can be implemented for the grid-side current just by changing the respective current feedback and reference.

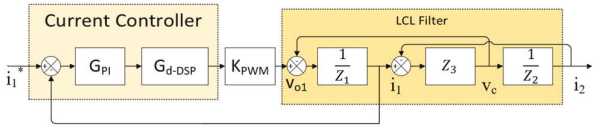

(a)

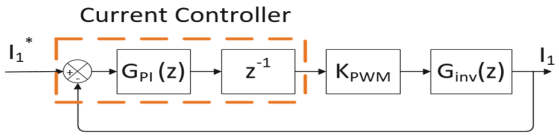

(b)

Fig. 2. Current control model (a) s-domain (b) z-domain.

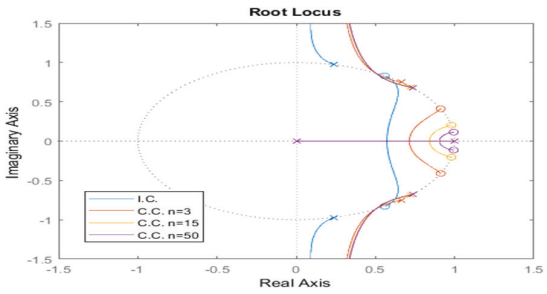

Fig. 3. Root loci of the inverter-side current for interactive (I.C) and common currents (C.C).

Considering the current controller from Fig. 2(b) and the result from (7), the closed-loop transfer function for the interactive and common currents are respectively given by:

$$C_{ij} = \frac{1}{n}\frac{G_{inv}(z)H}{(1+G_{inv}(z)H)}(i_{1i}^{*} - i_{1j}^{*}) \tag{14}$$

$$S_{i} = \frac{1}{n}\frac{G_{coupling\ inv}(z)H}{(1+G_{coupling\ inv}(z)H)}(i_{1i}^{*} - i_{1j}^{*}) \tag{15}$$

where

$$H = G_{PI}(z)z^{-1}K_{pwm}. \tag{16}$$

B. Stability Analysis for Inverter-Side Current Case

The system stability is determined by applying the root locus analysis to the open-loop forward path of (14) and (15). A system with multiple grid-connected inverters is only stable when the proportional gains of the current controllers are selected such that all values of the transfer functions for the interactive and common currents are inside the unit circle [6-7].

Furthermore, [2] showed that there is relation between a critical frequency of one sixth of the sampling frequency f_s and the LCL filter resonance f_{res} (or f_{res1}) that will determine whether the system can be stable for a single-loop feedback control. For the inverter-side current control, *the system will only be stable if the resonance frequency is less than the critical frequency* (i.e., $f_{res} < f_s/6$ and $f_{res1} < f_s/6$).

Fig. 3 shows the root loci of the interactive and common currents for the inverter-side feedback for different number of inverters using the parameters from the high-power microgrid testbed described in [9] and presented in Table I for convenience. The resonance frequency ω_{res} for the interactive current stability is calculated from (6) and the parameters in Table I. The LCL filter resonance frequency (1.52 kHz) is higher than the critical frequency (1.33 kHz), so the system is interactively unstable for the inverter-side current control. Fig. 3 corroborates this since the poles of the LCL filter are placed outside the unit circle for all values of the proportional gain for the interactive current.

However, there is a range where the system is stable for the common current due to a shift in the frequency of the poles and zeroes of the filter resonance and antiresonance frequencies. This stability range for selected number of inverters is given by:

TABLE I. SYSTEM PARAMETERS

Circuit Parameter	Formula	Nominal Value
Power Rating	S_b	2.0 MVA
Voltage Rating	V_b	480 V
Inverter-Side Inductor	L_1	20 µH
Grid-Side Inductor	L_2	12.2 µH
Filter Capacitor	C_f	Δ3x 480 µH
Resonance Frequency	f_r	1.52 kHz
Sampling Frequency	f_s	8 kHz
Critical Frequency	$f_s/6$	1.33 kHz

$$K_p Range = \begin{Bmatrix} 0 < K_p < 0.0709, n = 3 \\ 0 < K_p < 0.0822, n = 15 \\ 0 < K_p < 0.0844, n = 50 \end{Bmatrix}. \tag{17}$$

From (17), the stable range of the proportional gain increases as the number of inverters increases but converging towards a maximum value. Nonetheless, the entire system will always be unstable since the system is interactively unstable requiring additional damping when using the inverter-side currents.

Similarly, the LCL resonance frequency ω_{res1} for the common current stability can be calculated from (6). This equation shows that as the number of inverters increase, the resonance frequency decreases. For this reason, increasing the number of inverters could reduce the resonance frequency to a value lower than the critical frequency, making the system commonly stable for the inverter-side current.

Active Damping Control

A system using inverter-side current feedback with the critical frequency near the resonance frequency would require that the controller provides damping to move the poles of the resonance inside the unit circle. Proposed solutions for adding damping can be broadly classified in passive and active algorithms. The ESRs of the various components are normally small so they might not be able to make the system stable in high-power applications. Adding a passive resistor to damp the resonances introduces high power losses. Thus, the best solution is to use active damping algorithms which will reduce the resonances without introducing power losses [2, 10].

In this paper, the capacitor-voltage feedforward active damping algorithm is implemented [10-12]. The main reason for selecting this scheme is that no additional sensors are needed since the capacitor voltage is usually measured to synchronize the inverters with the grid through the phase-locked loop (PLL) algorithm. Moreover, reduction of large inrush currents during startup and suppression of the grid disturbances can be achieved using this active damping algorithm [11].

The block diagram of the dual-loop control system for the inverter-side current feedback with capacitor-voltage active damping is illustrated in Fig. 4. In this figure, K_{ff} is the gain of the feedforward control path, and $G_{cv}(z)$ is the transfer function of the capacitor voltage with respect to the inverter voltage, given by:

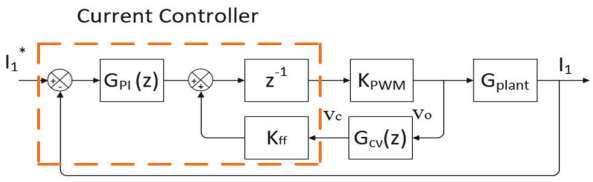

Fig. 4. Current control model in z-domain with capacitor-voltage feedforward active damping.

$$G_{cv}(s) = \frac{v_c(s)}{v_o(s)} = \frac{1}{L_1 C_f (s^2 + \omega_{res}^2)},$$

$$G_{cv}(z) = ZOH(G_{cv}(s)). \tag{18}$$

Considering the current controller with this active damping algorithm and the result from (7), the new closed-loop transfer functions for the interactive and common currents are the same ones as (14) and (15) but with a new transfer function for (16), given by:

$$H = \frac{G_{PI}(Z) z^{-1} K_{PWM}}{1 - z^{-1} K_{PWM} K_{ff} G_{cv}(z)}. \tag{19}$$

Using this equation, Fig. 5 shows the root loci of the interactive and common currents for the inverter-side current feedback using unit capacitor-voltage feedforward gain (i.e., $K_{ff} = 1$). Unlike the previous case, the poles of the system are now inside the unit circle for the interactive current. Thus, the system is interactively stable as long as the proportional gain is properly selected from 0 to 0.111. Similarly, the system will continue to have common current stability with a higher range of stability from K_p varying from 0 to 0.131. Applying this feedforward technique extends the limit of the resonance frequency up to one third of the sampling frequency (i.e., $f_r < f_s/3$) provided that:

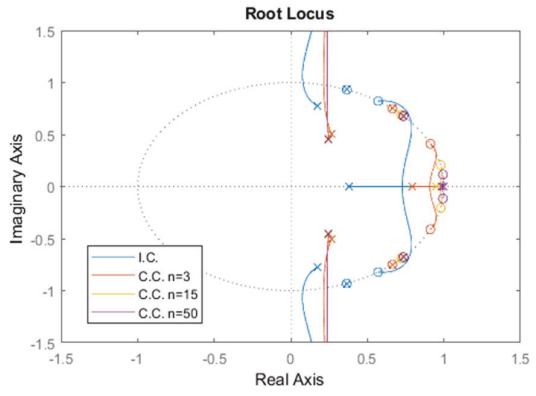

Fig. 5. Root loci of the interactive and common currents for inverter-side feedback with capacitor-voltage feedforward algorithm.

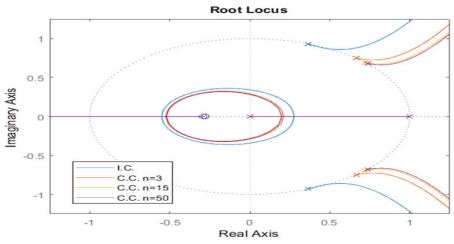

Fig. 6. Root loci of the grid-side current for interactive and common currents.

$$\cos(\omega_{res1} T_s) > -\frac{L_1}{2L_1 + 3(L_2 + nL_g)} \text{ [11].} \tag{20}$$

C. Stability Analysis for Grid-Side Current Case

A system with grid-side feedback will only be stable if the resonance frequencies of both the interactive and common currents are greater than the critical frequency (i.e., $f_{res} > f_s/6$ and $f_{res1} > f_s/6$) [2]. Following the same analysis as the case for the inverter-side feedback, it is expected that the system be interactively stable for the grid-side current since the resonance frequency is greater than the critical frequency. Moreover, it is expected that the system be commonly unstable because increasing the number of inverters decreases the resonance frequency f_{res1} to values lower than the critical frequency. In this case, the system will be unstable when only two inverters are added since the resonance frequency of the LCL filter is initially close to the critical frequency.

Fig. 6 shows the root loci analysis when using the grid-side current as feedback. In this case, the values that can be selected for the proportional gain to make the system interactively stable are within:

$$K_p Range = \{0 < K_p < 0.0653\}. \tag{21}$$

However, the system will be commonly unstable since the poles of the common current are located outside the unit circle regardless of the value of the proportional gain or the number of inverters. Therefore, the entire system is always unstable requiring additional damping. This shows that an inverter employing grid-side-current feedback is in risk of becoming unstable due to the movement of the resonance poles as more inverters are added to grid. Further examination of ω_{res1} shows that the resonance frequency will converge to a defined value. As the number of inverters increases, $nL_g >> L_2$ and $nL_g >> (L_1 + L_2)$. Thus, ω_{res1} will converge to:

$$\omega_{\min res1} = 2\pi f_{\min res1} = \sqrt{\frac{1}{L_1 C_f}}. \tag{22}$$

This means that if the minimum resonance frequency in (22) is greater than the critical frequency (i.e., $f_{min_{res1}} > f_s/6$), the system with grid-side current feedback will no longer be at risk of becoming commonly unstable regardless of the number of inverters in the grid.

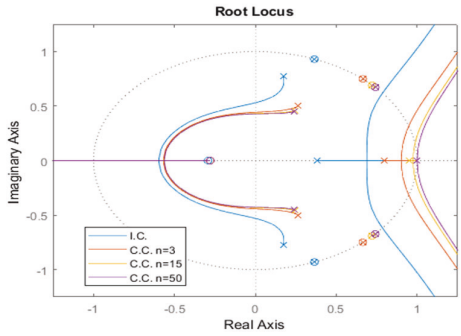

Fig. 7. Root loci of the interactive and common currents for grid-side feedback with capacitor-voltage feedforward algorithm.

Active Damping Control

Active damping will be applied to bring the poles of the system inside the unit circle since the system is unstable. Fig. 7 shows the root loci of the interactive and common currents for the grid-side-current feedback using the capacitor-voltage feedforward active damping shown in Fig. 4.

In this case, the system will continue to have interactive current stability with a higher range of stability from K_p varying from 0 to 0.101. Similarly, the poles for the common current are now inside the unit circle with a range of stability of:

$$K_p Range = \begin{Bmatrix} 0 < K_p < 0.087, n = 3 \\ 0 < K_p < 0.0832, n = 15 \\ 0 < K_p < 0.081, n = 50 \end{Bmatrix}. \quad (23)$$

Applying this feedforward technique changes the system stability range. As was the case with stability of the inverter-side current, the system will now be stable only if the resonance frequency is less than up to one third of the sampling frequency (i.e., $f_r < f_s/3$) and will become unstable if this limit is exceeded [12]. This means that unlike before, the system is no longer in risk of becoming unstable as more inverters are added to the grid since the maximum resonance frequency (1.52 kHz) is less than one third of the sampling frequency (2.67 kHz).

D. Filter Design Considerations on the System Stability

The previous sections have shown that the stability of the system will highly depend on the LCL filter resonance frequency. A LCL filter is usually designed to attenuate the overall ripple current amplitude, and the resonance frequency is selected to be less than half of the switching frequency f_{sw} and ten times greater than the fundamental frequency f_g (i.e., $10f_g < f_{res} (or\ f_{res1}) < 0.5f_{sw}$) [13]. This relation prevents the filter from amplifying switching noises and low order harmonics.

Fig. 8 illustrates the different ranges of stability of the system for the inverter- and grid-side current feedback considering the constrain imposed on the resonance frequency by the design guidelines of the LCL filter. Fig. 8 (a) and Fig. 8 (b) show the stability regions when the sampling frequency is

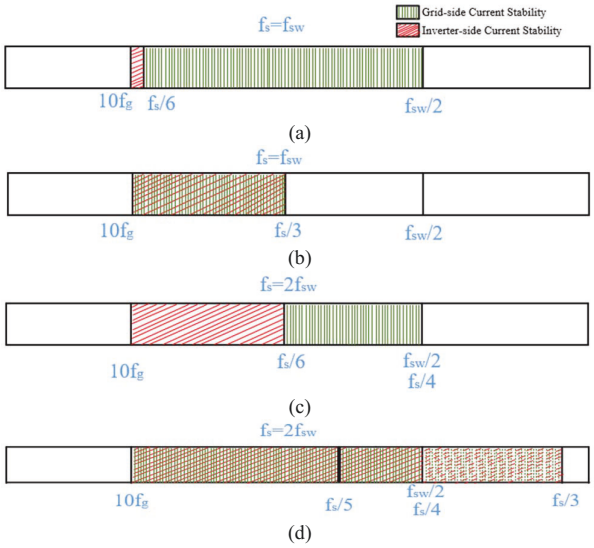

Fig. 8. Stability range for inverter- and grid-side current feedback for different cases: (a) fs =fsw without active damping (b) fs =fsw with active damping (c) fs =2fsw without active damping (d) fs =2fsw with active damping.

equal to the switching frequency (i.e., $f_s = f_{sw}$) for a system with and without the capacitor-feedforward algorithm. In this case, the grid-side current feedback will have a wider range of stability since it can be stable over the critical frequency with a single-loop controller and under twice the critical frequency with the implementation of the capacitor-voltage feedforward active damping.

Similarly, Fig. 8 (c) and Fig. 8 (d) show the stability regions when the sampling frequency is twice the switching frequency (i.e., $f_s = 2f_{sw}$) for a system with and without the capacitor-feedforward algorithm. In the system with the single-loop controller from Fig. 8 (c), the regions of stability are evenly distributed between the two feedback currents and the selection of the best feedback method will depend on the value of the filter resonance frequency. However, the system will always be stable when the capacitor-feedforward algorithm is implemented in Fig 8 (d) for both the inverter- and grid-side current feedback provided that the LCL filter had been properly designed.

Despite both feedback currents being stable in this situation, selecting the inverter-side current feedback is overall a better choice than the grid-side current. The main advantage being that no extra sensors are needed since the inverter-side current needs to be measured for switching device protection in high-power applications [1]. In addition, the previous analysis illustrated that the inverter-side current allows for higher values of the proportional gain near the critical frequency for both the interactive and common currents, which translates to a higher bandwidth and faster dynamics for the current controller. By iteratively changing the resonance frequency and examining the root loci, it was found that the inverter-side current feedback have a higher value for the proportional gain when the resonance frequency is lower than about one fifth of the sampling frequency (i.e., $10f_g < f_{res} < f_s/5$). This means that as

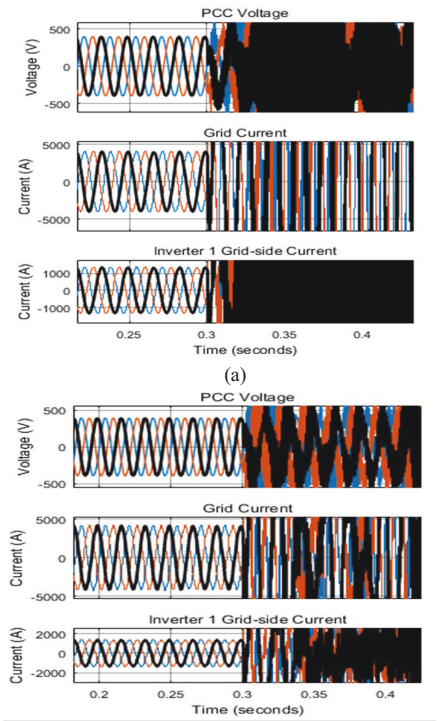

Fig. 9. Current waveforms for (a) inverter-side current feedback (b) grid-side current feedback.

the sampling frequency increases, this range increases, as well. Conversely, the grid-side current feedback will always have a fixed range of $f_s/5 < f_{res} < f_s/4$. Thus, the inverter-side current will have a wider range where the value of proportional gain can be selected higher than the value of gain for the grid-side current.

IV. Similations Results

In order to validate the effects of the active damping algorithm based on feedforward-unity capacitor voltage with both the inverter- and grid-side currents as feedback, MATLAB/SIMULINK™ is used to model a system consisting of three 2-MVA grid-connected parallel inverters feeding the power grid. All three inverters are set to inject 800 kW to the grid. The capacitor voltage feedforward technique is initially used in both cases and is turned off for all inverters at t = 0.3 s.

Fig. 9 (a) shows that using the inverter-side current as feedback, the systems becomes unstable as the capacitor voltage feedforward term is turned off because the interactive current is unstable. Similarly, Fig. 9 (b) reveals that using the grid-side current as feedback, the system becomes unstable as the capacitor voltage feedforward term is turned off because the common current is unstable. As mentioned before, the LCL filter resonance frequency utilized in these cases is very close to the critical frequency and therefore, both cases are unstable without active damping.

V. Conclusions

This paper performed a stability analysis considering the proportional gain of the current controller for multiple parallel- and grid-connected inverters using the inverter- and grid-side currents as feedback signals. Modeling of the inverter- and grid-side current feedback using the current separation method was performed. Moreover, the system stability range for both feedback-current approaches with and without active damping based on capacitor-voltage feedforward was examined using the root locus analysis, and those ranges of stability were examined considering the limitations given by the LCL filter design procedure. Overall, the analysis revealed that grid-side current feedback is a better choice when the the sampling frequency is the same as the switching frequency because of its wider range of stability. However, the inverter-side current is better when the sampling frequency is twice the switching frequency due to mainly no needing additional sensors. Finally, the theoretical analysis was validated through simulations.

Acknowledgments

The authors are grateful to the financial support from the NSF I/UCRC Grid-Connected Advanced Power Electronic Systems (GRAPES) under grant IIP-1439700.

References

[1] Y. Liu, C. Farnell, V. Jones, K. George, H. A. Mantooth and J. C. Balda, "Resonance propagation of ac filters in a large-scale microgrid," 2015 IEEE 6th International Symposium on Power Electronics for Distributed Generation Systems (PEDG), Aachen, 2015, pp. 1-6. doi: 10.1109/PEDG.2015.7223078

[2] S. G. Parker, B. P. McGrath and D. G. Holmes, "Regions of Active Damping Control for LCL Filters," in IEEE Transactions on Industry Applications, vol. 50, no. 1, pp. 424-432, Jan.-Feb. 2014. doi: 10.1109/TIA.2013.2266892

[3] Y. Tang, P. C. Loh, P. Wang, F. H. Choo, F. Gao, "Exploring Inherent Damping Characteristic of LCL-Filters for Three-Phase Grid-Connected Voltage Source Inverters," IEEE Trans. Power Electron., vol. 27, no. 3, pp. 1433-1443, Mar. 2012.

[4] Y. Liu, C. Farnell, H. A. Mantooth, J. C. Balda, R. A. McCann and C. Deng, "Resonance propagation modeling and analysis of AC filters in a large-scale microgrid," 2016 IEEE Applied Power Electronics Conference and Exposition (APEC), Long Beach, CA, 2016, pp. 143-149. doi: 10.1109/APEC.2016.7467865

[5] J. Dannehl, C. Wessels and F. W. Fuchs, "Limitations of Voltage-Oriented PI Current Control of Grid-Connected PWM Rectifiers With LCL Filters," in IEEE Transactions on Industrial Electronics, vol. 56, no. 2, pp. 380-388, Feb. 2009. doi: 10.1109/TIE.2008.2008774

[6] M. Lu, X. Wang, P. C. Loh and F. Blaabjerg, "Resonance Interaction of Multiparallel Grid-Connected Inverters With LCL Filter," in IEEE Transactions on Power Electronics, vol. 32, no. 2, pp. 894-899, Feb. 2017. doi: 10.1109/TPEL.2016.2585547

[7] M. Lu, X. Wang, P. C. Loh and F. Blaabjerg, "Interaction and aggregated modeling of multiple paralleled inverters with LCL filter," 2015 IEEE Energy Conversion Congress and Exposition (ECCE), Montreal, QC, 2015, pp. 1954-1959. doi: 10.1109/ECCE.2015.7309936

[8] J. L. Agorreta, M. Borrega, J. López and L. Marroyo, "Modeling and Control of N -Paralleled Grid-Connected Inverters With LCL Filter Coupled Due to Grid Impedance in PV Plants," in IEEE Transactions on Power Electronics, vol. 26, no. 3, pp. 770-785, March 2011. doi: 10.1109/TPEL.2010.2095429

[9] Y. Liu, C. Farnell, J. C. Balda and H. A. Mantooth, "A 13.8-kV 4.75-MVA microgrid laboratory test bed," 2015 IEEE Applied Power

Electronics Conference and Exposition (APEC), Charlotte, NC, 2015, pp. 697-702. doi: 10.1109/APEC.2015.7104426

[10] M. Lu, Z. Xin, X. Wang, R. N. Beres and F. Blaabjerg, "Extended stable boundary of LCL-filtered grid-connected inverter based on an improved grid-voltage feedforward control," 2016 IEEE Energy Conversion Congress and Exposition (ECCE), Milwaukee, WI, 2016, pp. 1-7. doi: 10.1109/ECCE.2016.7855103

[11] X. Li, J. Fang, Y. Tang, X. Wu and Y. Geng, "Capacitor-Voltage Feedforward With Full Delay Compensation to Improve Weak Grids Adaptability of LCL-Filtered Grid-Connected Converters for Distributed Generation Systems," in IEEE Transactions on Power Electronics, vol. 33, no. 1, pp. 749-764, Jan. 2018. doi: 10.1109/TPEL.2017.2665483

[12] M. Lu and F. Blaabjerg, "Stability identification for grid-connected inverters with LCL filters considering grid-voltage feedforward regulator," 2017 IEEE 18th Workshop on Control and Modeling for Power Electronics (COMPEL), Stanford, CA, 2017, pp. 1-5. doi: 10.1109/COMPEL.2017.8013342

[13] A. Reznik, M. G. Simões, A. Al-Durra and S. M. Muyeen, "LCL Filter Design and Performance Analysis for Grid-Interconnected Systems," in IEEE Transactions on Industry Applications, vol. 50, no. 2, pp. 1225-1232, March-April 2014. doi: 10.1109/TIA.2013.2274612